

1. Laboratory of Seismology and Physics of Earth's Interior, University of Science and Technology of China
 2. Department of Geosciences, State University of New York at Stony Brook

1. INTRODUCTION

As a typical active intracontinental mountain range in Central Asia, Tian Shan Mt serves as the prototype in studying geodynamic processes and mechanism of intracontinental mountain building. We study 3D crust and the uppermost mantle structure beneath Tian Shan and close region using ambient noise and earthquake surface waves.

2. DATA AND METHODS

My data set contains 60 broad-band seismic stations mainly located at foot of Tian Shan mountain and joint area. Several stations, situated at the southern foot of Altai Mt. and northern foot of Kunlun Mt., provide critical ray path coverage of Junggar and Tarim basins. Our dataset includes vertical component continuous record from 2015 to 2016 and teleseismic waveforms, whose magnitudes are over 5.5, focal depths are shallower than 200 km and happened during 2013 and 2016.

Firstly, we measure group velocity dispersion curve of fundamental-mode Rayleigh wave in the period of 3 to 45 s using a frequency-time analysis method from two-year stacked Empirical Green's Function (EGF). Secondly, we collect surface wave data from teleseismic events and measure group velocities of the fundamental-mode of Rayleigh wave in the period of 25 to 55 s using a two-station method. Finally, we combine the group velocity dispersion curves measured from ambient noise and earthquake surface waves, obtain lateral isotropic group velocity maps at different periods based on tomography and invert a 3D Vsv model of crust and uppermost mantle down to about 70 km using a Monte Carlo Inversion method.

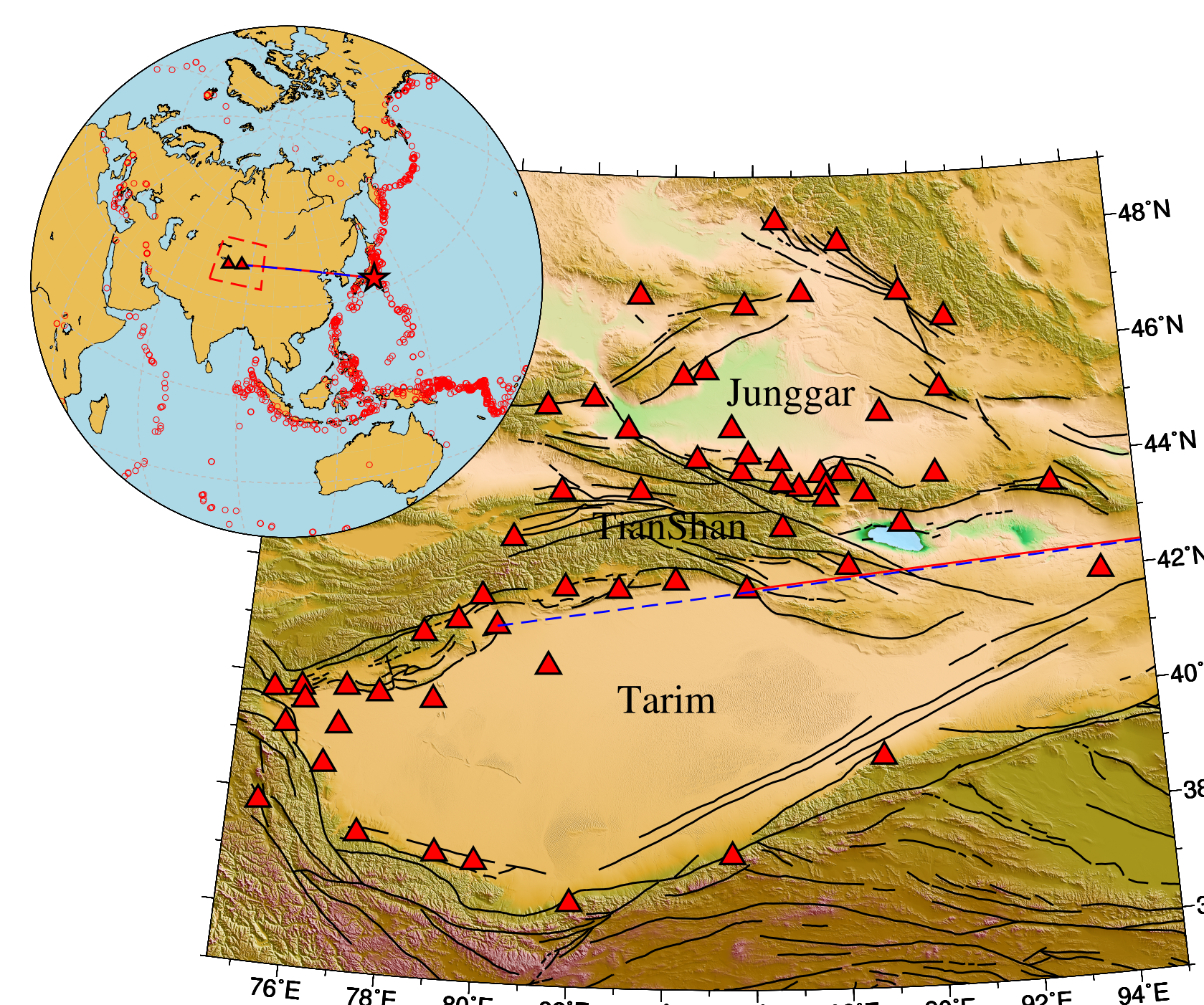


Fig. 1. Map of research area. Red triangles represent broad-band seismic stations in Tianshan area used in this study. Solid black thick lines show the faults. The insert (top left) depicts telsesimic distribution. Red circles represent epicenter of teleseismic used in this study, which happened from 2013 to 2016. Dashed red square is study area. Two triangles represent two stations named as AKS and KOL, which are in common line with this star-labelled earthquake.

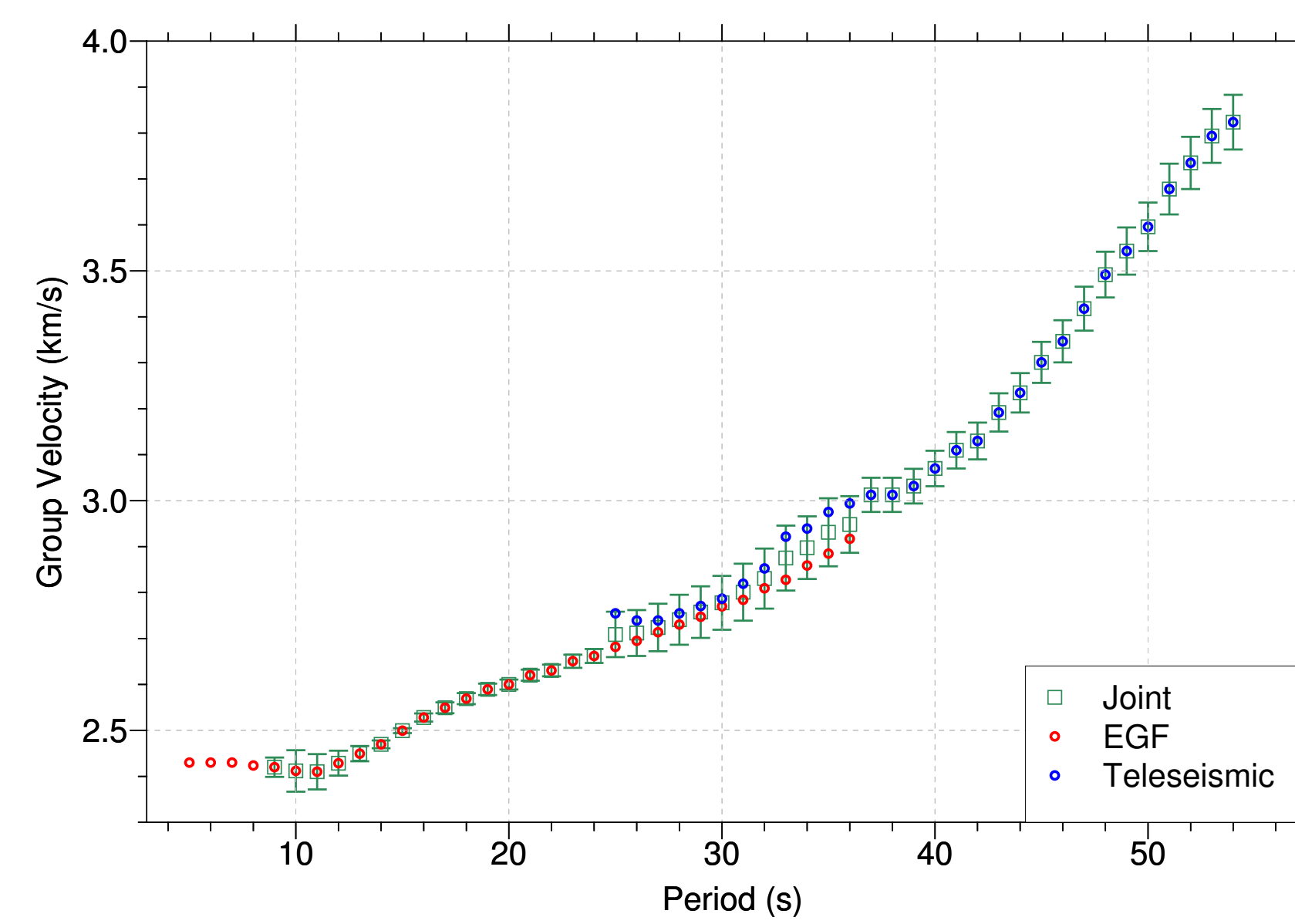


Fig. 2. Demos of combination of group velocity dispersion curves between two stations, AKS and KOL. Red circles denote dispersion points measured from EGF while blue circles represent those measured from teleseismic. Limegreen squares give combined dispersion curve. At overlap periods, green squares are weight average of blue and red circles, in which weights are inverse of their error which summation of their errors gives error of combined dispersion curve.

3. 2D GROUP VELOCITY MAPS

In this section, we present inverted 2D group velocity maps.

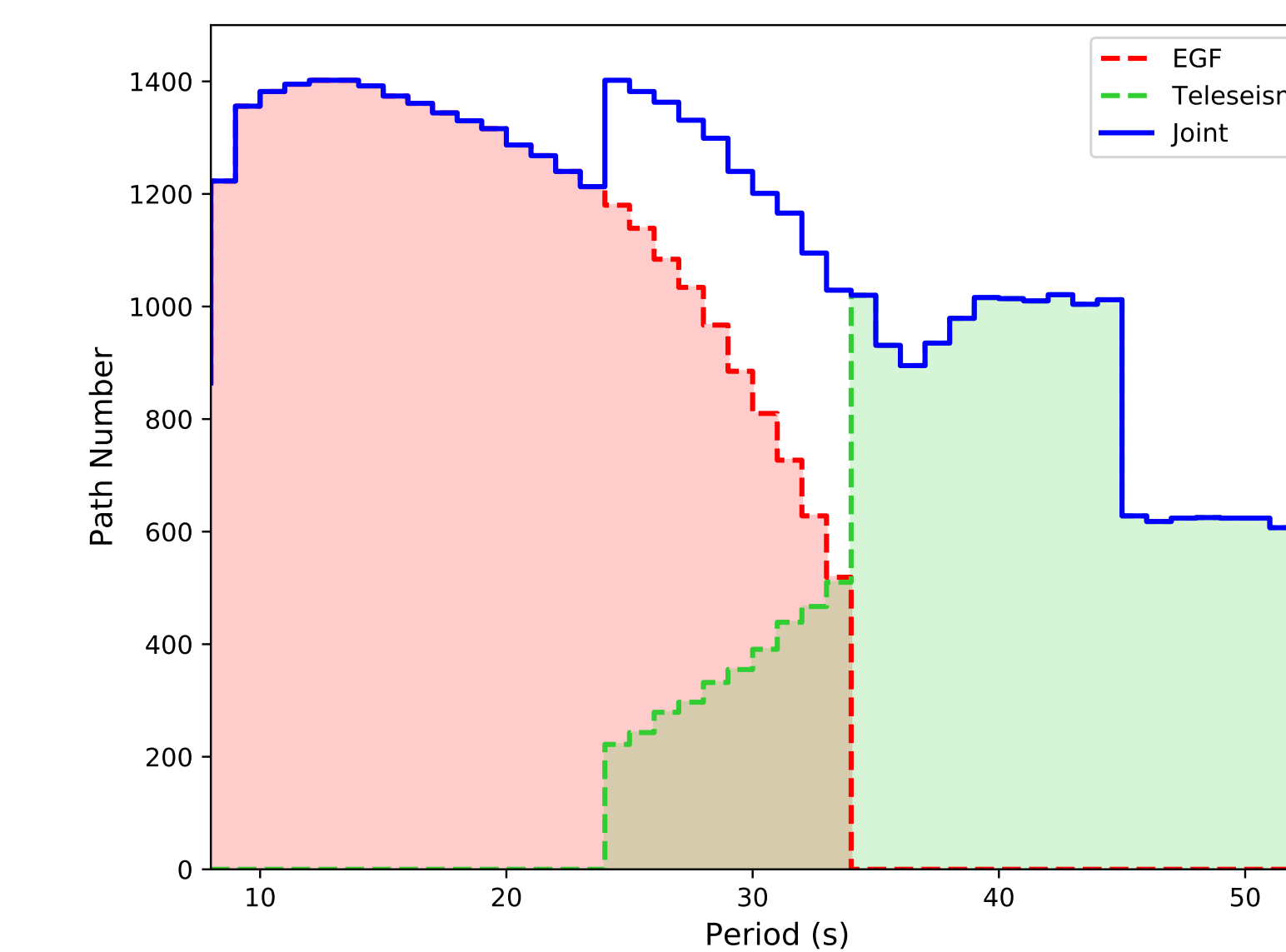


Fig. 3. Dispersion curve numbers used for tomography, variate with period. The Dashed limegreen line and corresponding limegreen area shows number of used dispersion curves measured from teleseismic with two-station method while Dashed red line and area denote number of those measured from EGF at each period. The solid blue line indicates numbers of all used dispersion curves which are summation of above two.

The PKiKP-PcP differential travel time residuals exhibits large spatial variations from -1.0 s to 1.0 s in a horizontal distance of about 5° (Fig. 2).

The PKiKP-PcP differential travel time residuals have a positive correlation with PKiKP travel time residuals (Fig. 3a), while no correlation is found with PcP travel time residuals (Fig. 3b), implying that the large variations of PKiKP-PcP residuals mainly come from PKiKP phases. A typical ULVZ model of a 10% decrease in P wave velocity over a 15 km layer near the PKiKP entrant or exit points at the CMB, gives a travel time perturbation of about 0.12 s, which is not quite large enough to account for the observed variation of 1.0 s. Thus, the observed PKiKP-PcP differential travel time residuals may indicate a ICB topographic change of 5 km.

Fig. 3. Relationship among PKiKP-PcP differential travel time residuals, PKiKP travel time residuals and PcP travel time residuals. Events are coded using different colors.

The binned PKiKP/PcP amplitude ratios exhibit much larger values than predictions of different ICB models (Fig. 4) and spatial variations (Fig. 5).

Fig. 4. Observed PKiKP/PcP amplitude ratios (dots) as a function of epicentral distance, with predictions (lines) of different P wave speed (a) and density (b) contrasts across the ICB. The red squares represent average amplitude ratios of each bins, and the error bar represent standard deviations.

Fig. 5. Binned PKiKP/PcP amplitude ratio residuals, defined as the ratio between observed and predicted PKiKP/PcP amplitude ratios. 1° geographical bins with the bin centers shift by 1° in latitude and longitude are used. The ratio residuals are plotted at the mean PKiKP reflection locations in each bins.

4. ICB BENEATH THE BEARING SEA

In this section, we present seismic observations which sample the ICB region beneath Bearing Sea (Fig. 1b). The small variations of the PKiKP-PcP differential travel time residuals indicate a flat ICB in this region (Fig. 6).

The linear relationship between PKiKP and PcP travel time residuals (Fig. 7) indicates that most variations in PKiKP and PcP travel time residuals originate from shallow Earth's heterogeneity, which can be effectively eliminated by using PKiKP-PcP differential travel time residuals.

Fig. 7. Relationship among PKiKP-PcP differential travel time residuals, PKiKP travel time residuals and PcP travel time residuals.

The stacked PKiKP and PcP waveforms show similar waveforms (Fig. 8), indicating a sharp interface at both the CMB and ICB. The PKiKP/PcP amplitude ratios exhibit large scattering on single records. The PKiKP/PcP amplitude ratios binned by epicentral distance, exhibit much larger amplitude ratios than predictions of different ICB models (Fig. 9).

Fig. 8. Comparisons of stacked PKiKP (blue) and PcP (black) waveforms in each geographical bins. The locations of the bins center and the number of traces used in each stacking are labeled at the right of each traces.

Fig. 9. Observed PKiKP/PcP amplitude ratios (dots) as a function of epicentral distance, with predictions (lines) of different P wave speed (a) and density (b) contrasts across the ICB. The red squares represent average amplitude ratios in each bins, and the error bar represent standard deviations.

5. CONCLUSIONS

We collect a large dataset of high-quality PKiKP waveforms, and use PKiKP-PcP differential travel time residuals, PKiKP/PcP amplitude ratios, and PKiKP-PcP waveform differences to constrain ICB properties. Based on the observations, the ICB beneath Bearing Sea has a sharp and flat boundary, and the ICB beneath Mexico may have a bumpy ICB with a topographic height change of 5 km. PKiKP/PcP amplitude ratios are much larger than predictions, implying possible other factors which affects the amplitude ratios.